

# Deployment-complete benchmarking

El Mustapha Mansouri<sup>1,\*</sup>, Keigo Arai<sup>1</sup>

<sup>1</sup>School of Engineering, Institute of Science Tokyo, Yokohama, Kanagawa 226-8501, Japan

\*Correspondence: [mansouri.e.2224@m.isct.ac.jp](mailto:mansouri.e.2224@m.isct.ac.jp)

## Abstract

Benchmarks increasingly guide deployment, procurement and scientific screening, yet a score supports only the response it records, not necessarily the deployment action. We introduce deployment-complete benchmarking, which tests whether benchmark evidence determines a deployment action. A benchmark is complete for a claim exactly when the action is constant on each evidence fiber; mixed fibers expose missing deployment information, and completion curves quantify the evidence required to resolve ambiguity. In controlled response spaces, benchmark-channel conformal coverage of 94.98% transferred poorly to an unmeasured deployment channel (10.07%), whereas response-rank intervals achieved 94.91% coverage; even zero benchmark error certified only 45.4% of candidates at the largest residual size. Public audits revealed incompleteness, including 97.9% mixed Tox21 fibers and zero median certifiable fraction in main Matbench and JARVIS audits. In held-out replays, certify-then-acquire reduced false decisions from 1.19% to 0.027% in Tox21 and from 20.3% to 0.128% in JARVIS, while changing model choice and identifying deployment-relevant probes. Deployment-ready benchmarks should report evidence, supported actions, ambiguity and completion cost rather than scores alone.

Benchmarks rank models, guide procurement and increasingly determine which systems are trusted outside the test set. A score therefore often becomes evidence for an action: deploy a model, advance a material, triage a compound or decide which expensive measurement to acquire next.

But a benchmark score is evidence only for the response it records. Deployment may depend on another response, such as robustness, safety, toxicity, stability or a thresholded physical property. A model can be accurate, calibrated and competitive on the benchmark while the action made from that score remains underdetermined.

We introduce deployment-complete benchmarking. A benchmark records evidence  $E : \mathcal{S} \rightarrow \mathcal{Z}$ , and a deployment claim is an action  $D : \mathcal{S} \rightarrow \mathcal{A}$ . Here  $\mathcal{S}$ ,  $\mathcal{Z}$  and  $\mathcal{A}$  denote candidates, evidence and actions. The benchmark is complete for the claim when candidates with the same evidence require the same action, equivalently  $D = \phi \circ E$ . Mixed fibers are witnesses of missing deployment information.

This gives a diagnostic, a limit and a design rule. The diagnostic is the mixed-fiber audit; the limit is that no statistic computed from the same evidence can complete a missing-response claim; the design rule is the completion curve, which measures the cost of acquiring the information needed to support the action. Across controlled spaces, public audits and held-out replays, benchmark accuracy, calibration and uncertainty can leave deployment actions unresolved; completion evidence reduces false decisions, changes model choice and identifies the missing response to measure.

## Results

### **Benchmark evidence determines only some deployment claims**

Deployment-complete benchmarking turns the benchmark-to-deployment step into an auditable property of a report (Fig. 1). A benchmark records an evidence map  $E : \mathcal{S} \rightarrow \mathcal{Z}$ , while the deployment claim is an action  $D : \mathcal{S} \rightarrow \mathcal{A}$ . The benchmark is claim-complete for  $D$

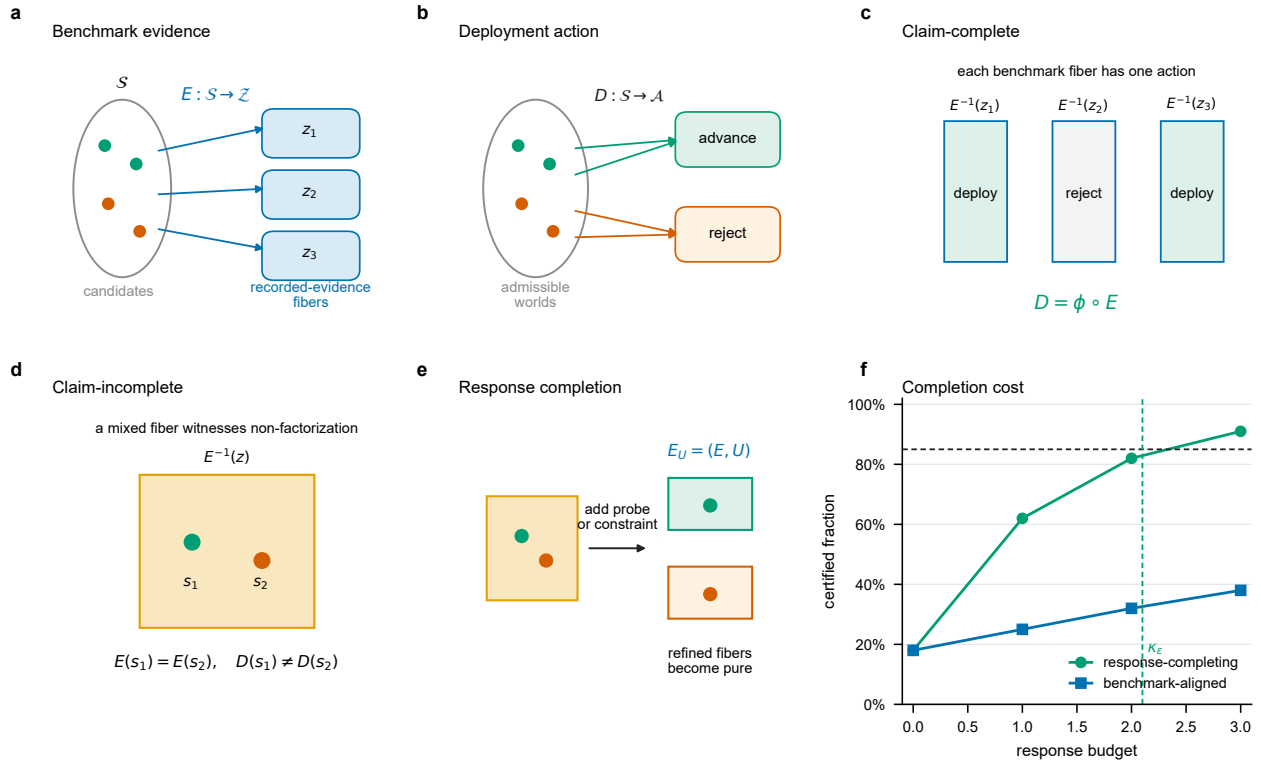


Figure 1: **Deployment-complete benchmarking tests whether benchmark evidence supports an action.** **a**, A benchmark report records an evidence map  $E : \mathcal{S} \rightarrow \mathcal{Z}$  that partitions candidates into fibers. **b**, A deployment claim specifies an action  $D : \mathcal{S} \rightarrow \mathcal{A}$  that may depend on responses outside the score. **c**, The benchmark is claim-complete when the action is constant on every evidence fiber, equivalently  $D = \phi \circ E$ . **d**, A mixed fiber containing benchmark twins with different deployment actions witnesses missing evidence. **e**, Adding a response probe or trusted constraint  $U$  refines the evidence map to  $E_U = (E, U)$  and can make fibers pure. **f**, Completion curves report the certified fraction as a function of response budget; the completion cost  $\kappa_\epsilon$  is the budget needed to reach a target certified fraction.

exactly when the action is constant on every benchmark fiber. Equivalently,  $D = \phi \circ E$ . A mixed fiber is therefore a mathematical witness that the reported evidence package does not yet support the claim.

**Proposition 1** (Claim-completeness diagnostic). *Let  $E : \mathcal{S} \rightarrow \mathcal{Z}$  be benchmark evidence and  $D : \mathcal{S} \rightarrow \mathcal{A}$  a deployment action. The following are equivalent:  $D$  is determined by benchmark evidence;  $D$  is constant on every fiber  $E^{-1}(z)$ ; there exists a map  $\phi : \mathcal{Z} \rightarrow \mathcal{A}$  such that  $D = \phi \circ E$ ; and no two benchmark-indistinguishable admissible worlds require different deployment actions.*

Evaluation object	Question answered	What remains unresolved
Accuracy or leaderboard	Which model predicts recorded labels best?	Whether the recorded labels determine the deployment action
Calibration or conformal prediction	Are predictions reliable for the calibrated response?	Whether another response or action is covered
Uncertainty or out-of-distribution (OOD) detection	Is the input, prediction or representation unusual?	Whether ordinary evidence fibers contain multiple actions
Active learning	Which label would improve a model?	Which response makes the deployment action decidable
Deployment-complete benchmarking	Is the action a function of benchmark evidence?	The completion cost of unresolved claims

Table 1: **Deployment-complete benchmarking evaluates a different object from standard benchmark summaries.** Conventional evaluation objects remain useful for ranking, reliability and data acquisition. Completion asks whether the evidence package supports the action being claimed and what response information remains missing.

The consequence is a benchmark reporting standard. A deployment-facing benchmark should not report a score alone; it should report the action the score is meant to support, the evidence map used to support it, the fraction of candidates whose action is already determined and the completion cost of the remaining ambiguity. This turns leaderboard evaluation into an evidence-design problem.

A statistic computed only from the same declared evidence cannot repair non-factorization. If  $T = h(E)$  and  $D$  does not factor through  $E$ , then  $D$  cannot factor through  $T$ , because  $D = \psi \circ h \circ E$  would imply factorization through  $E$ . This applies to leaderboard scores, calibration summaries or uncertainty summaries only when they are functions of  $E$  alone. Methods using new measurements, descriptors, model internals, auxiliary labels or structural assumptions refine the evidence map instead of repairing non-factorization by scoring.

The resulting comparison with standard evaluation objects is simple (Table 1): they measure performance or reliability for a recorded response, whereas deployment completeness asks what actions the evidence package supports.

The design object is the completion curve: the supported fraction of deployment claims

as a function of additional evidence budget. In finite audits this is the fraction of pure augmented-evidence fibers; in modeled response spaces it is the corresponding declared certificate. Thus a benchmark is deployment-ready not when its score is high, but when its completion cost is low for the claim being made. The loss-aware and linear-response versions of this construction are given in Methods.

## Perfect benchmark evidence can leave deployment incomplete

Benchmark-channel conformal prediction retained 94.98% coverage on measured labels but only 10.07% on the deployment channel; at the largest residual size, exact benchmark responses still certified only 45.4%. We isolated this mechanism in a synthetic response space whose geometry is known. Benchmark probes spanned three effective dimensions, while the deployment probe varied from nearly in-span to mostly out-of-span. In this controlled response-space experiment,  $Y_*(c)$  is the deployment response for candidate  $c$ ,  $\hat{y}_c$  its benchmark-based center,  $g$  the benchmark-null residual size,  $R_c$  the admissible fiber radius and  $\delta_c$  the benchmark-channel error bound. Across 50 geometries and data seeds, an oracle conformal predictor calibrated on deployment labels recovered 94.42%, and response-rank intervals using the residual term achieved 94.91% (Fig. 2a). As the residual size  $g$  grew, benchmark-calibrated deployment coverage collapsed while response-rank intervals stayed near nominal coverage (Fig. 2b). The conformal result shows response specificity: conformal intervals cover the response channel on which they are calibrated, while deployment coverage requires deployment-channel calibration or a residual-response certificate. Mahalanobis OOD scores and bootstrap uncertainty were likewise nearly uncorrelated with the completion gap because they measured input novelty or benchmark-channel variance rather than the benchmark-null deployment direction.

The failure is not merely lower accuracy; it persists at zero benchmark error. Setting the benchmark-channel error term to zero removes  $\delta_c$  from the interval, but the residual term

remains:

$$|Y_*(c) - \hat{y}_c| \leq R_c g.$$

Thus exact knowledge of the measured benchmark response still leaves completion cost whenever the deployment direction has a benchmark-null component and the admissible fiber has positive radius. With  $\delta_c = 0$ , the certified fraction fell from 100% at  $g = 0$  to 69.9% at  $g = 0.5$  and 45.4% at  $g = 1.0$ ; completing the response direction kept certification at 100% (Fig. 2d).

The same geometry produced a leaderboard inversion. Model A had the best benchmark mean absolute error (MAE) but certified only 6% of its top-100 candidates; Model E had worse benchmark MAE but certified all top-100 candidates because its response span covered the deployment probe (Fig. 2c). Across 50 runs, the best-MAE model was not the best-certifying model in all structured runs and in 72% of equal-noise null runs. A benchmark can therefore reward a model specialized to measured response coordinates while penalizing one that spans directions needed for deployment.

Completion can also come from trusted structure rather than direct measurement of the deployment response. In a nonlinear constrained-fiber experiment, benchmark evidence alone led to false decisions on 15.0% of candidates; an ambient response-rank certificate certified 16.1% with zero false certificates. Adding the valid constraint  $h \approx \sin(\pi b)$ , where  $b$  is scalar benchmark evidence and  $h$  is an unobserved hidden response coordinate, refined the admissible set and raised certification to 97.0% with zero false certificates.

## Completion reduces false decisions and changes model choice

The consequence is not only residual ambiguity: in a representative JARVIS split, the benchmark-MAE model made 613 false band-gap decisions and the response-selected certify-and-acquire workflow made none. More generally, if benchmark evidence does not determine the deployment action, benchmark actions can make false decisions. Exact finite audits certify

released candidate sets; operational replays estimate fibers from calibration data and apply them to held-out candidates, so they measure empirical policy risk rather than mathematical zero-error certification on an unobserved population.

In Tox21, a benchmark-fiber majority policy decided every held-out compound and made empirical false SR-p53 decisions on 1.19% of candidates (10th–90th percentile, 1.00–1.37%). A conservative response-certification rule with minimum support 50 decided 0.66% immediately and sent the rest to SR-p53 acquisition; after acquisition, the empirical false-decision rate was 0.027% (0.00–0.18%). In JARVIS, formation-energy predictions were the benchmark observable and band-gap energy ( $E_{\text{gap}} > 1.0 \text{ eV}$ ) was the deployment claim. Across 15 public models and 50 held-out splits per model, local benchmark-majority action made empirical false band-gap decisions on 20.3% of candidates (19.2–21.6%). The response-certification rule immediately decided 2.46%, sent the rest to acquisition and reduced empirical false decisions to 0.128% (0.00–0.29%; Fig. 3). Model choice also changed: benchmark MAE always selected an exact-MAE formation-energy model, whereas response-certified held-out behaviour selected a different model in all 50 splits.

We converted the replay into a costed deployment decision, measuring costs in units of one false deployment decision and charging acquisition for each ambiguous candidate. In JARVIS, certify-then-acquire avoided 562.2 false band-gap decisions per split on average and remained lower-cost whenever one band-gap acquisition cost less than 20.7% of a false deployment decision (10th–90th percentile, 19.5–21.9%). Tox21 avoided 25.6 false decisions per split and broke even below 1.18% (1.00–1.37%). An asymmetric loss sweep weights false positives and false negatives separately and reduces to these break-even values when the two costs are equal. Ambiguous candidates are not failures in this workflow; they are acquisition requests when benchmark evidence does not determine the deployment response.

The next section traces these operational failures to the fiber structure of reported benchmark evidence across domains.

## Released evidence leaves mixed deployment fibers across domains

Across public audits the pattern was systemic: Tox21 had 97.9% mixed seven-assay fibers, and the main 20-quantile Matbench/JARVIS audits had 0% median certifiable fraction. The purpose of these audits is not to show that distinct scientific properties differ. It is to explain why evidence actually released or scored by a benchmark can fail in the operational replays above. A mixed fiber, or benchmark twin, is a pair of candidates with the same reported evidence but different deployment actions. Tox21 has exact binary assay fibers, spin-defect screening has reported substrate completions, the vision audit uses finite clean-prediction fibers, and Matbench Discovery and JARVIS require declared finite-resolution fibers for continuous predictions. The domain-specific scored evidence maps and fiber rules are specified in Supplementary Table 1.

Across this range, mixed fibers were common. In the lightweight vision sanity check, clean prediction, clean correctness and decile-binned clean confidence left a median 22.7% of corruption-robustness claims ambiguous across eight classifiers and 25 splits<sup>1</sup>. In Tox21, seven nuclear-receptor assays were the benchmark response and SR-p53 the deployment endpoint<sup>2</sup>, producing the 97.9% mixed-fiber rate above. In spin-defect screening, bare-host coherence was the benchmark response and substrate viability the deployment claim<sup>3-6</sup>; 43 of 187 valid hosts (23.0%) were response-ambiguous.

We also computed a loss-aware ambiguity score: the Bayes error of the best fiber-wise benchmark-only action, normalized by the global majority-action error. This prevalence-normalized residual ambiguity was 0.65 in vision, 0.85 in Tox21 and 0.98 as a conservative spin-defect lower bound, so the mixed fibers are not merely visual artifacts of label imbalance.

Materials-property leaderboards showed the same pattern. Under the main 20-quantile released-prediction audit, the median certifiable fraction was 0% for both Matbench Discovery stability labels across 67 public prediction files and JARVIS band-gap threshold labels across 15 public models<sup>7-9</sup>. Sensitivity analyses over quantile resolution, nearest-neighbour fibers and calibration-error windows showed the same qualitative conclusion: released formation-energy

predictions alone left the stability and band-gap threshold claims largely unresolved at the declared finite resolutions (Fig. 4c). Under the main 20-quantile rule, normalized residual ambiguity was 1.00 for Matbench and 0.89 for JARVIS. These audits isolate released-response evidence, not richer descriptors, domain models or auxiliary measurements.

## Locked completion selects the deployment-relevant probe

In the locked label-blinded JARVIS replay, one completion-selected probe decided 72.0% of held-out band-gap cases with 0.54% empirical false decisions, versus 15.1% with 3.69% for benchmark-aligned or uncertainty policies. It selected real modified Becke–Johnson (MBJ) band gap in every split, while benchmark-aligned and uncertainty policies selected the formation-energy-like control (Fig. 5). Completion curves select response information that makes an action decidable, not merely measurements that are uncertain, diverse or benchmark-aligned. In the controlled response space, three residual-greedy probes raised certification from 45.8% to 70.8%, outperforming uncertainty or diversity (47.8%), benchmark-aligned sampling (54.0%) and random sampling (59.3%; Fig. 5). Predicted residual reduction tracked realized completion gain across probes (Pearson  $r = 0.976$ ), whereas benchmark alignment did not ( $r = -0.029$ ).

In Tox21, response-rank selected SR-MMP then SR-HSE as completion probes for the held-out SR-p53 action. One and two added assays decided 5.64% and 6.58% of held-out compounds, above uncertainty, random, diversity and benchmark-aligned baselines; label permutation reduced the gain. A supervised selective baseline showed how richer evidence legitimately changes the map: with only the seven benchmark assays it decided 1.55% of held-out compounds, whereas adding simplified molecular-input line-entry system (SMILES) descriptors decided 92.0% with 0.95% empirical false decisions.

In a cost-weighted JARVIS companion pool, completion per cost selected a low-cost residual probe in 92.0% of splits, while benchmark-aligned acquisition selected the cheap formation-energy-like probe.

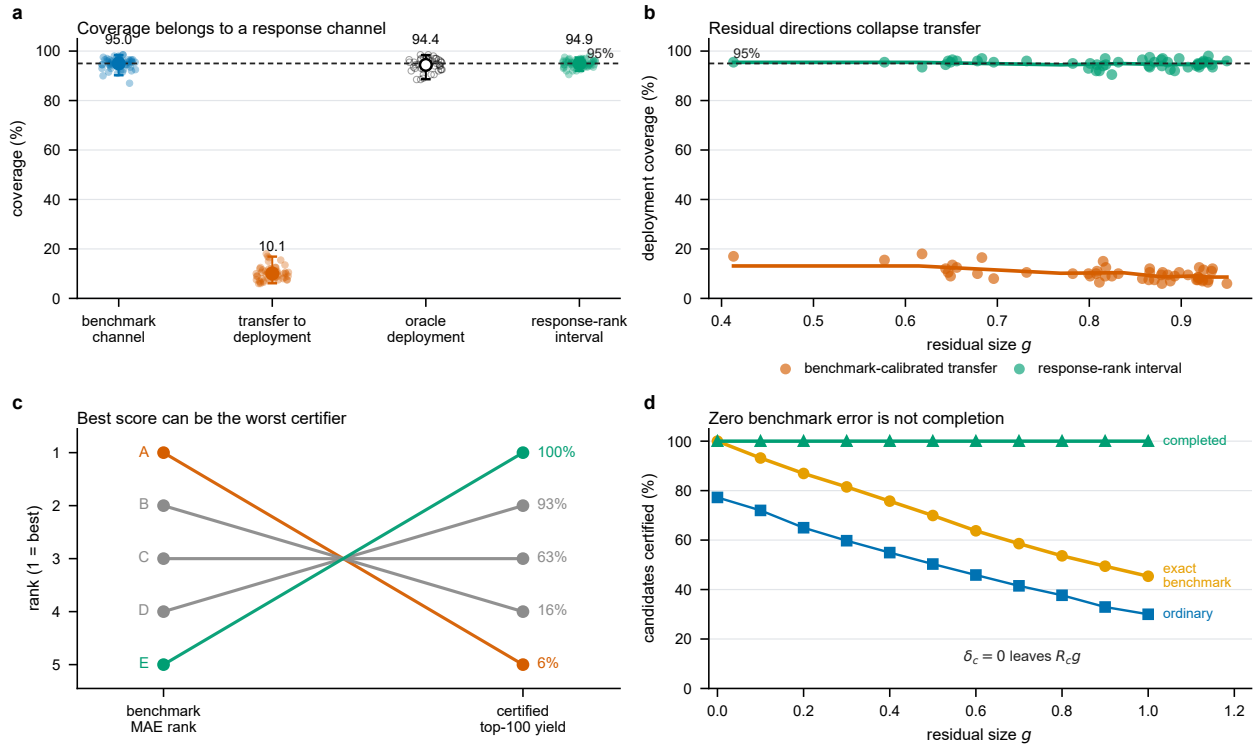
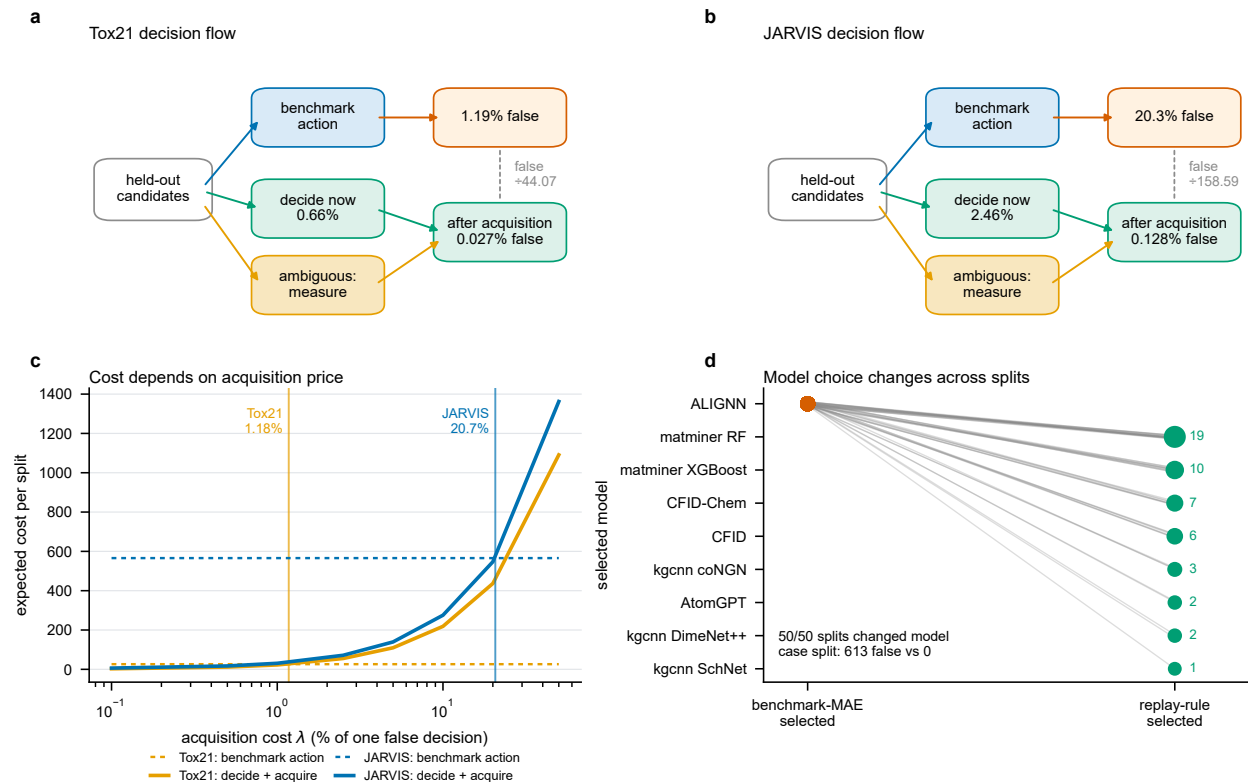


Figure 2: **Perfect benchmark evidence can leave deployment incomplete.** **a**, Benchmark-channel conformal coverage does not transfer to an unmeasured deployment response, whereas response-rank intervals recover nominal coverage without deployment calibration labels. Points show 50 repeated geometries/seeds; centre markers show means and error bars show 2.5–97.5 percentile ranges; dashed line marks 95% nominal coverage. **b**, Deployment coverage under benchmark-calibrated transfer falls as the residual response component grows, while response-rank intervals remain near 95% across the same 50 runs. **c**, A leaderboard inversion over 50 repeated model-ranking runs: the best benchmark-MAE model is the worst certifier of top deployment candidates. **d**, Zero benchmark error removes  $\delta_c$  but not residual ambiguity in the controlled negative control: when  $g > 0$ , exact benchmark responses still leave the  $R_c g$  term, whereas response completion keeps the claim certified.



**Figure 3: Completion reduces false decisions and reverses model choice.** **a**, In 100 held-out Tox21 splits, the response-certification rule plus acquisition of ambiguous fibers reduces empirical false SR-p53 decisions from 1.19% to 0.027%. **b**, In JARVIS, 50 held-out splits for each of 15 public models show that the response-certification rule plus acquisition reduces empirical false band-gap decisions from 20.3% to 0.128%. **c**, Expected cost as a function of acquisition cost, with break-even points at 1.18% for Tox21 and 20.7% for JARVIS. **d**, Across JARVIS splits, formation-energy MAE and replay-certified yield select different models; in a representative split, the benchmark-MAE model makes 613 false band-gap decisions whereas the response-selected certify-and-acquire workflow makes none. Nonzero false decisions arise from the immediately decided calibration-certified subset; ambiguous candidates are deferred to acquisition and are not counted as benchmark-supported decisions. Split intervals summarize replay variability over repeated partitions of the same finite datasets rather than independent population confidence intervals.

**a**

Cross-domain evidence map

domain	Benchmark observable	Deployment claim	Fiber rule	Ambiguous	Next response
Vision	clean prediction	corruption robust	finite prediction	22.7%	corruptions
Tox21	7 assays	SR-p53	exact assay pattern	97.9%	SR-p53
Spin defects	bare host	substrate viability	reported substrates	23.0%	substrate
Matbench	formation energy	stability	quantile / kNN / window	100% main audit	stability
JARVIS	formation energy	band gap	quantile / kNN / window	100% main audit	band gap

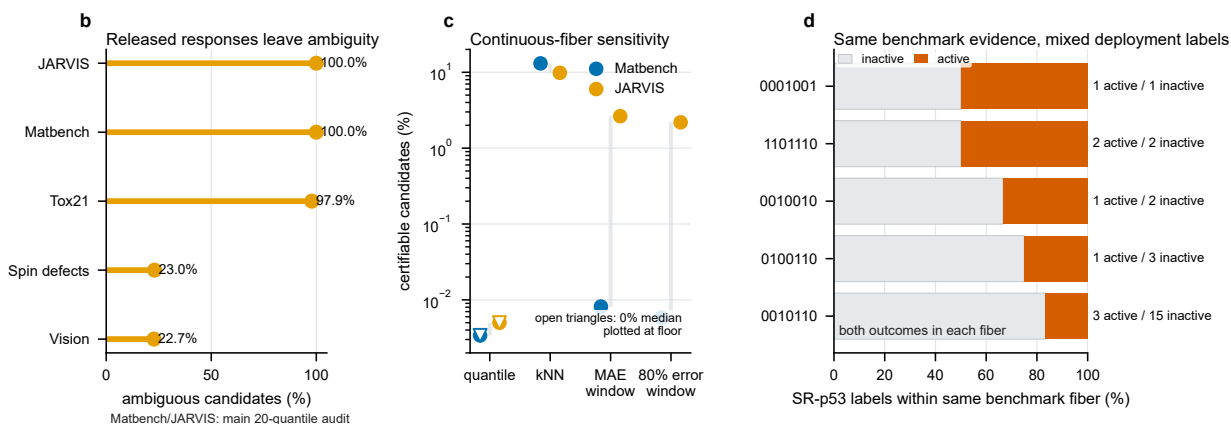


Figure 4: **Released evidence leaves mixed deployment fibers across domains.** **a**, Evidence maps linking each benchmark observable to the deployment claim, fiber rule, ambiguity fraction and next response. **b**, Ambiguous fractions across vision, toxicology, spin-defect screening and materials benchmarks. Matbench and JARVIS use the main 20-quantile released-prediction audit; panel c summarizes finite-resolution sensitivity. **c**, Low certifiable fractions persist under quantile, nearest-neighbour and model-specific prediction-error windows; open triangles mark true 0% medians plotted at the log-scale floor. Full sensitivity values are reported in Supplementary Table 2. **d**, Tox21 example showing identical seven-assay benchmark evidence with mixed SR-p53 labels.

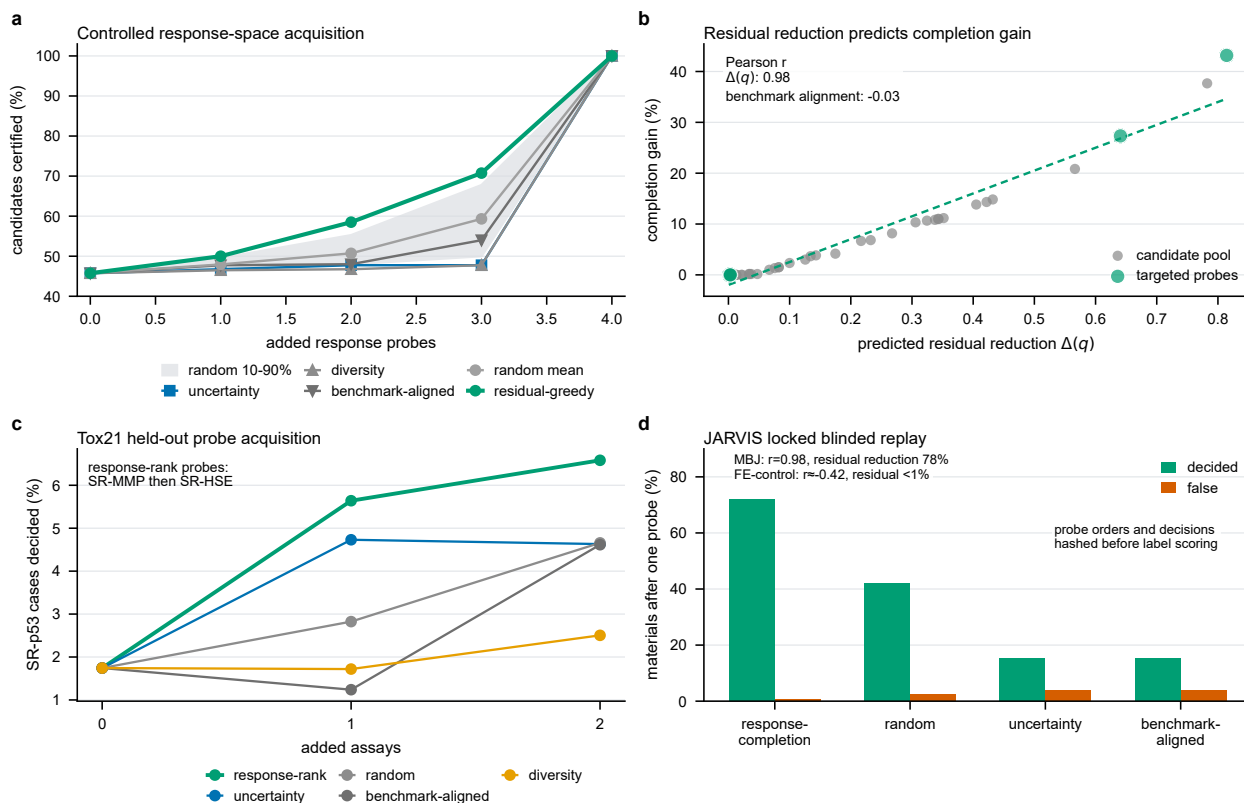


Figure 5: **Locked completion selects the deployment-relevant probe.** **a**, In the controlled response space, residual-greedy acquisition certifies more candidates than uncertainty, diversity, benchmark-aligned or random sampling; points show policy means over 50 seeds. **b**, Across candidate probes for a single declared deployment response, the predicted residual reduction  $\Delta(q)$  tracks realized completion gain, while benchmark alignment does not. **c**, In held-out Tox21 probe acquisition over 200 random splits, response-rank selects SR-MMP first and SR-HSE second, deciding more SR-p53 cases under the calibration-certification rule than baselines after one or two added assays. **d**, Locked, label-blinded JARVIS replay over 200 calibration/test splits. Bars show calibration-certified held-out decisions after one added probe; false portions are empirical false decisions among all held-out candidates after the locked rule. Response-completion selects real MBJ band gap and decides 72.0% with 0.54% empirical false decisions; benchmark-aligned and uncertainty policies select a synthetic formation-energy-like control and decide 15.1% with 3.69% empirical false decisions.

## Discussion

Deployment-complete benchmarking changes the unit of evaluation from a score to a score–claim pair. A benchmark score becomes meaningful for deployment only after specifying the action it is meant to support and the evidence through which the benchmark observes candidates. The factorization condition gives an exact diagnostic for this relationship; completion curves quantify the cost of repairing it when it fails. The output is an auditable evidence package: score, evidence map, supported action, ambiguous fraction, completion curve and next measurement.

Accuracy, calibration, conformal prediction, uncertainty estimation, out-of-distribution detection and active learning remain valuable, but they answer different questions: ranking, reliability, novelty or label efficiency for a measured response. Completion asks whether the evidence package determines the action. This connects benchmark reporting to sufficiency and experiment comparison [10,11](#), partial identification [12–14](#), value-of-information and optimal design [15–18](#), as well as property elicitation, robust decision-making and selective classification [19–30](#).

The experiments show why this standard matters. In controlled response spaces, zero benchmark error and valid benchmark-channel conformal coverage do not imply deployment-channel completeness. Across modalities, reported benchmark evidence leaves mixed fibers and residual deployment risk. In Tox21 and JARVIS replays, completion-aware policies select different measurements, reduce false decisions, defer ambiguous cases to acquisition and can change model choice. The framework is evidence-relative by design: descriptors, model internals, auxiliary labels, physical constraints or prospective measurements change the evidence map and can lower completion cost. For benchmarks used in deployment, procurement or scientific screening, reports should state the score, evidence map, supported action, ambiguous fraction, completion curve and remaining acquisition cost.

# Methods

**Certification terminology.** We use three certification terms. Exact certification refers to finite released-set fibers whose deployment labels are known and pure; this is a deterministic statement about the declared candidate set. Calibration certification refers to a rule learned from calibration fibers and applied to held-out candidates; it produces an empirical false-decision rate and is not a formal zero-error population guarantee. Predicted certification refers to interval or residual-radius rules derived from declared modeling assumptions. All held-out replay results are calibration-certified policy evaluations unless explicitly labelled exact finite certifications.

**Claim-completeness and finite fibers.** Let  $\mathcal{S}$  be an admissible system class, let  $E : \mathcal{S} \rightarrow \mathcal{Z}$  be the declared benchmark evidence map and let  $D : \mathcal{S} \rightarrow \mathcal{A}$  be the deployment action. The evidence-compatible fiber at  $z$  is  $\mathcal{C}_z = \{s \in \mathcal{S} : E(s) = z\}$ . The benchmark is claim-complete for  $D$  on a fiber when  $D$  is constant on  $\mathcal{C}_z$ . The factorization theorem follows from the standard quotient argument. If  $D = \phi \circ E$ , then  $E(s_0) = E(s_1)$  implies  $D(s_0) = \phi(E(s_0)) = \phi(E(s_1)) = D(s_1)$ , so  $D$  is constant on benchmark fibers. Conversely, if  $D$  is constant on each nonempty fiber, choose any  $s_z \in E^{-1}(z)$  and define  $\phi(z) = D(s_z)$ . The definition is well-defined because the fiber is pure, and  $\phi(E(s)) = D(s)$  for every  $s \in \mathcal{S}$ . The indistinguishability statement is the same condition written contrapositively. Score-invariance is immediate: if a statistic computed only from the declared benchmark evidence has the form  $T = h(E)$  and  $D = \psi \circ T$ , then  $D = \psi \circ h \circ E$ , so  $D$  would factor through  $E$ . For cost-sensitive actions with state-dependent deployment loss  $L(a, s)$ , this can be relaxed to an  $\epsilon$ -robust fiber condition

$$\inf_{a \in \mathcal{A}} \sup_{s \in \mathcal{C}_z} \left\{ L(a, s) - \inf_{a' \in \mathcal{A}} L(a', s) \right\} \leq \epsilon.$$

In finite audits with candidates  $i = 1, \dots, N$ , the exact certifiable fraction is

$$\text{Cert}(E, D) = \frac{1}{N} \sum_z |\mathcal{C}_z| \mathbf{1}\{D \text{ is constant on } \mathcal{C}_z\}, \quad \text{Amb}(E, D) = 1 - \text{Cert}(E, D).$$

For binary deployment actions, we also report the fiber Bayes error of the best benchmark-only decision rule,

$$\text{Err}(E, D) = \frac{1}{N} \sum_z |\mathcal{C}_z| \min\{p_z, 1 - p_z\}, \quad p_z = \Pr(D = 1 \mid E = z),$$

and the prevalence-normalized residual ambiguity

$$\rho(E, D) = \frac{\text{Err}(E, D)}{\min\{\Pr(D = 1), \Pr(D = 0)\}}.$$

Here  $\rho = 0$  means the declared evidence completes the binary action, whereas  $\rho = 1$  means the best evidence-fiber action has the same error as the global majority rule for a proper partition. For  $k$ -nearest-neighbour (kNN) and error-window sensitivity, neighbourhoods overlap rather than partition the candidate set, so the reported decision-risk column is a local-neighbourhood majority error and normalized values can slightly exceed one. The spin-defect value is reported as a conservative lower-bound risk because the public file records substrate completions rather than a full candidate-by-substrate binary table. For a scalar deployment response  $Y_\star : \mathcal{S} \rightarrow \mathbb{R}$  and threshold  $\tau$ , define  $D_\tau(s) = \mathbf{1}\{Y_\star(s) > \tau\}$ . A fiber is certified positive when  $\inf_{s \in \mathcal{C}_z} Y_\star(s) > \tau$ , certified negative when  $\sup_{s \in \mathcal{C}_z} Y_\star(s) \leq \tau$  and ambiguous when the threshold cuts through the fiber. A mixed fiber directly witnesses non-factorization.

**Completion cost.** Let  $\mathcal{Q}$  be a set of possible response probes and let  $E_U(s) = (E(s), \{q(s) : q \in U\})$  be the evidence after adding  $U \subseteq \mathcal{Q}$ . With additive probe costs  $\text{cost}(U) = \sum_{q \in U} c_q$ ,

the ideal completion curve is

$$\Gamma_E(b; D) = \max_{U \subseteq \mathcal{Q}: \text{cost}(U) \leq b} \text{Cert}(E_U, D),$$

and the  $\epsilon$ -completion cost is

$$\kappa_\epsilon(E, D) = \inf\{b : \Gamma_E(b; D) \geq 1 - \epsilon\}.$$

Exact optimization can be combinatorial; the experiments therefore report completion curves under specified policies and compare them with oracle, uncertainty, diversity, benchmark-aligned and random baselines.

The loss-aware analogue uses action-label loss  $\ell$  and replaces pure-fiber counting with Bayes risk. For a population distribution on  $\mathcal{S}$ , define

$$R(E, D; \ell) = \inf_{\phi: \mathcal{Z} \rightarrow \mathcal{A}} \mathbb{E}\{\ell(\phi(E(S)), D(S))\}.$$

For augmented evidence  $E_U$ , the expected value of evidence is

$$\Delta_\ell(U) = R(E, D; \ell) - R(E_U, D; \ell),$$

and a cost-aware completion objective is

$$V_\ell(U) = R(E_U, D; \ell) + \text{cost}(U).$$

The one-step expected value of information for a probe  $q$  after already measuring  $U$  is

$$\text{EVI}(q | U) = R(E_U, D; \ell) - R(E_{U \cup \{q\}}, D; \ell).$$

Exact claim-completeness is the zero-risk special case  $R(E, D; \ell_{0/1}) = 0$  under 0–1 deployment

loss.

**Linear response-rank specialization.** Let  $\mathcal{H}$  be a Hilbert space of response functions or latent response states. Benchmark probes  $k_1, \dots, k_m \in \mathcal{H}$  define evidence  $E_B(s) = (\langle k_1, s \rangle, \dots, \langle k_m, s \rangle)$  and span  $B = \text{span}\{k_1, \dots, k_m\}$ , with orthogonal projector  $P_B$ . A deployment response is  $Y_\star(s) = \langle k_\star, s \rangle$ . If  $k_\star \in B$ , then  $Y_\star$  is a linear function of benchmark evidence. If  $k_\star \notin B$ , let

$$r_\star = (I - P_B)k_\star, \quad g = \|r_\star\|.$$

Then  $r_\star \neq 0$ ,  $\langle k_j, r_\star \rangle = 0$  for each benchmark probe and, for any scalar  $t \neq 0$ , the two worlds  $s_0 = 0$  and  $s_1 = tr_\star$  have identical benchmark evidence but different deployment response:

$$Y_\star(s_1) - Y_\star(s_0) = t\|r_\star\|^2 \neq 0.$$

Thus  $g$  is the norm of the deployment direction invisible to the benchmark. A nonzero residual is an algebraic invisibility diagnostic in the ambient response space. Claim-incompleteness on a particular admissible set  $\mathcal{S}$  additionally requires either an explicit pair  $s_0, s_1 \in \mathcal{S}$  with equal benchmark evidence and different deployment action, or a declared feasible-fiber radius that permits variation in the residual direction. When physical, causal or policy constraints shrink feasible fibers, the relevant quantity is the feasible deployment-response diameter, not the ambient residual norm alone.

**Feasible-fiber and interval bounds.** Let  $\mathcal{S} \subset \mathcal{H}$  be an admissible system class and let  $b = (b_1, \dots, b_m)$  be a benchmark evidence vector. The set  $\mathcal{C}_b = \{s \in \mathcal{S} : \langle k_j, s \rangle = b_j, j = 1, \dots, m\}$  is the corresponding benchmark fiber. For any  $s, s' \in \mathcal{C}_b$ ,

$$|\langle k_\star, s' - s \rangle| \leq g \|s' - s\|,$$

because  $s' - s$  is benchmark-null and Cauchy–Schwarz gives  $|\langle r_\star, s' - s \rangle| \leq g \|s' - s\|$ . If the admissible class contains the radius- $R$  step  $s + Rr_\star/\|r_\star\|$ , benchmark measurements are

unchanged and the deployment response changes by  $Rg$ . Physical constraints may shrink the feasible fiber, in which case the exact ambiguity is the feasible-fiber diameter rather than the ambient Hilbert-ball diameter.

If benchmark-channel prediction error is bounded by  $\delta_c$  and candidate  $c$  has admissible benchmark-null radius  $R_c$ , every compatible perturbation  $u \perp B$  with  $\|u\| \leq R_c$  satisfies

$$|\langle k_\star, u \rangle| = |\langle r_\star, u \rangle| \leq R_c g,$$

so

$$|Y_\star(c) - \hat{y}_c| \leq \delta_c + R_c g.$$

Here  $\hat{y}_c$  is the benchmark-based center, or predicted deployment response, for candidate  $c$ . The diagnostic forms  $I_c = [\hat{y}_c - (\delta_c + R_c g), \hat{y}_c + (\delta_c + R_c g)]$  and certifies a threshold action only when  $I_c$  lies wholly on one side of the threshold.  $R_c$  is declared before certification from replicate measurement variation, simulation/model discrepancy, validation fibers or domain tolerance.

**One-step response completion.** For a candidate response probe  $q$ , let  $q_\perp = (I - P_B)q$ . If  $q_\perp = 0$ , the probe lies inside the existing benchmark span and cannot reduce the residual. Otherwise the updated residual after adding  $q$  is

$$r_\star(q) = r_\star - \frac{\langle r_\star, q_\perp \rangle}{\|q_\perp\|^2} q_\perp,$$

so

$$g(q)^2 = \|r_\star(q)\|^2 = g^2 - \frac{\langle r_\star, q_\perp \rangle^2}{\|q_\perp\|^2}.$$

The squared residual reduction is therefore

$$\Delta(q) = \frac{\langle r_\star, q_\perp \rangle^2}{\|q_\perp\|^2},$$

and the cost-normalized greedy completion probe is

$$q^* = \arg \max_{q \in \mathcal{Q}} \frac{\langle r_\star, q_\perp \rangle^2}{\|q_\perp\|^2 c_q}.$$

The selected probe is appended to the benchmark set, intervals are recomputed and candidate classes updated. Radius sensitivity multiplied all  $R_c$  by 0.5, 0.75, 1.0, 1.25, 1.5 and 2.0.

**Local nonlinear extension.** For differentiable response models  $y_k(x) = \langle k, f_\theta(x) \rangle$ , let  $J_B(x)$  be the matrix of benchmark gradients and  $P_{J_B}$  the projector onto its row span. Define  $g_J = \|(I - P_{J_B})\nabla y_\star(x)\|$ . If  $\|\nabla^2 y_\star\|_2 \leq L_\star$  in  $\|\Delta x\| \leq R_c$ , then every local benchmark-null direction  $J_B(x)\Delta x = 0$  satisfies

$$|y_\star(x + \Delta x) - y_\star(x)| \leq R_c g_J + \frac{1}{2} L_\star R_c^2.$$

For benchmark channel  $j$  with Hessian bound  $\|\nabla^2 y_j\|_2 \leq L_j$  on the same neighbourhood, tangent-null leakage is bounded by  $\frac{1}{2} L_j R_c^2$ . The nonlinear ablation used NumPy tanh networks with input dimension 12, output dimension 8, hidden width 32, depths 1, 2, 4 and 6, and 50 random initializations per depth. Gradients were computed exactly by backpropagation and local Hessian envelopes were estimated from random directions. Outputs are `nonlinear_linearization_ablation.csv` and its summary file.

**Controlled experiments.** The response-channel transfer experiment used an 8-dimensional response space, four benchmark probes of effective rank 3, label noise  $\sigma = 0.05$  and split conformal prediction with  $\alpha = 0.05$ . OOD detection used Mahalanobis distance and uncertainty used a 50-member bootstrap ensemble. Repeated summaries used 50 seeds. The leaderboard experiment used a 10-dimensional response space, deployment probe  $k_\star = (e_0 + \dots + e_7)/\sqrt{8}$  and five model spans of rank 3, 4, 6, 7 and 8. Structured and equal-noise repetitions are written to `revision_leaderboard_repeated_summary.csv`. The decision-sufficiency generalization experiment used 100 seeds with 1,000 candidates per seed. The benchmark

evidence was  $b \in [-1, 1]$ , the deployment response was  $y_\star = b + 0.9h$  with threshold  $\tau = 0.4$ , and the admissible hidden coordinate satisfied  $h = \sin(\pi b) + u$ ,  $u \in [-0.12, 0.12]$ . The ambient response-rank certificate used only  $h \in [-1.2, 1.2]$ . Outputs are cached in the `outputs/` directory with the prefix `decision_sufficiency`. The zero-benchmark-error control fixed the same certification rule while setting  $\delta_c = 0$  and sweeping  $g \in [0, 1]$ ; the residual-reduction control evaluated each candidate probe against one declared deployment response and compared the theoretical  $\Delta(q)$  with realized certified-fraction gain. Outputs are `zero_benchmark_error_control.csv`, `residual_reduction_completion_gain.csv` and `residual_reduction_completion_gain_summary.csv`.

**Operational replays.** The replay script used held-out calibration/deployment splits and should be read as an empirical risk evaluation of a completion-aware policy. In Tox21, 100 random splits used 50% calibration compounds to define seven-assay fibers and their calibration SR-p53 labels to estimate fiber purity; 50% held-out compounds were then used to evaluate SR-p53 decisions. A held-out fiber could certify only if it had at least 50 calibration compounds and a single calibration SR-p53 label. More generally, for a calibration fiber  $z$  with  $n_z$  examples and empirical disagreement rate  $\hat{p}_z$ , a calibration-certified rule can require a one-sided upper confidence bound  $p_z^+$  to satisfy  $p_z^+ \leq \tau$ . With zero observed disagreements, the Clopper–Pearson bound is  $p_z^+ = 1 - \delta_z^{1/n_z}$ ; allocating  $\delta_z = \delta/m$  across  $m$  tested fibers gives simultaneous conditional error control under exchangeability within fibers. The operational replays use the simpler unanimous-support rule and report held-out empirical risk; the confidence-bound version is the corresponding finite-sample calibration certificate. Under a Bernoulli interpretation without multiplicity correction, 50 unanimous labels exclude discordance rates above  $1 - 0.05^{1/50} = 5.8\%$  at 95% confidence. In JARVIS, 50 splits per model used formation-energy prediction windows with half-width equal to calibration MAE; a held-out material was certified only when all calibration materials in its window shared the same band-gap threshold label.

The costed replay paired each benchmark-action row with the corresponding certify-then-

acquire row. Benchmark action incurred one unit for every false deployment decision. Certify-then-acquire incurred the same false-decision cost plus  $\lambda$  units for every ambiguous candidate sent to acquisition. The reported break-even acquisition cost is  $(E_{\text{benchmark}} - E_{\text{certify+acquire}})/A$ , where  $E$  is the number of false decisions and  $A$  is the number of acquired ambiguous candidates. This symmetric convention is the special case of an asymmetric deployment-loss calculation. If  $C_{\text{FP}}$  and  $C_{\text{FN}}$  are false-positive and false-negative costs and  $C_{\text{acq}}$  is the cost of acquiring the missing response for one deferred candidate, then

$$L_{\text{bench}} = C_{\text{FP}} \text{FP}_{\text{bench}} + C_{\text{FN}} \text{FN}_{\text{bench}},$$

whereas

$$L_{\text{comp}} = C_{\text{FP}} \text{FP}_{\text{comp}} + C_{\text{FN}} \text{FN}_{\text{comp}} + C_{\text{acq}} N_{\text{defer}}.$$

Completion is lower-cost whenever

$$C_{\text{acq}} < \frac{C_{\text{FP}}(\text{FP}_{\text{bench}} - \text{FP}_{\text{comp}}) + C_{\text{FN}}(\text{FN}_{\text{bench}} - \text{FN}_{\text{comp}})}{N_{\text{defer}}}.$$

Figure 3 reports the symmetric case  $C_{\text{FP}} = C_{\text{FN}} = 1$ . The asymmetric sweep over  $C_{\text{FP}}/C_{\text{FN}} \in [0.1, 10]$  is written to `asymmetric_cost_break_even.csv` and plotted in `asymmetric_cost_heatmap.pdf`. Case studies were chosen from held-out splits by the largest difference between the certified error of the benchmark-MAE model and the certification-selected model.

The Tox21 response-probe acquisition campaign used the same complete-label compounds, the same SR-p53 deployment endpoint and the same minimum support of 50 calibration compounds. The initial response panel was the seven nuclear-receptor assays; the candidate probes were SR-ARE, SR-ATAD5, SR-HSE and SR-MMP. For each of 200 random splits, policies chose probes using calibration compounds and calibration SR-p53 labels only, then scored held-out compounds after the probe order was fixed. The response-rank policy chose the assay that maximized the supported pure SR-p53 fiber fraction on calibration data; the oracle chose the as-

say that maximized held-out certification and is reported only as an upper bound. The permutation control used the same splits but permuted calibration SR-p53 labels for probe selection only; after the probe order was frozen, certificate maps were built from real calibration labels and evaluated on held-out compounds. Outputs are `tox21_probe_permutation_control.csv` and `tox21_probe_permutation_control_summary.csv`.

The Tox21 deployment-label selective baseline used the same 100 calibration/test splits and the same held-out SR-p53 endpoint. We trained logistic-regression classifiers on calibration SR-p53 labels with two evidence maps: the seven nuclear-receptor assays alone, and those assays plus SMILES character  $n$ -gram descriptors (2–4 grams, capped at 2,048 features). A held-out compound was decided when the predicted class probability exceeded a declared confidence threshold; otherwise it was deferred. Thresholds 0.5, 0.6, 0.7, 0.8, 0.9 and 0.95 were evaluated. Outputs are `tox21_selective_baseline.csv` and `tox21_selective_baseline_summary.csv`. This baseline is an evidence refinement using deployment labels and richer descriptors, not a statistic of the original seven-assay evidence map.

The JARVIS label-blinded probe-completion experiment used the 187 materials present in all three JARVIS-Leaderboard reference files for formation energy per atom, optB88vdW (optimized Becke88 van der Waals) band gap and MBJ hybrid-functional band gap. The deployment label was band-gap energy ( $E_{\text{gap}} > 1.0$  eV; 33.7% viable). Candidate probes were a real JARVIS MBJ band-gap response (real JARVIS density-functional-theory (DFT) calculation,  $r = 0.98$  with the deployment target) and a synthetic formation-energy-correlated control response (formation energy plus Gaussian noise with standard deviation  $0.3\sigma_{\text{fe}}$ , where  $\sigma_{\text{fe}}$  is the formation-energy standard deviation, mimicking a benchmark-aligned measurement). In each of 200 calibration/test splits (70/30), the policy chose the probe from calibration materials only. The chosen probe, held-out material decisions and campaign manifest were then written to JSON and hashed before held-out optB88vdW labels were scored. Certification used 2-D quantile fibers (8 bins per dimension, minimum fiber size 3). This replay is a response-channel validation experiment rather than a cost claim about MBJ as the universally appropriate

measurement; in a real screening workflow, the completion probe depends on simulation or measurement cost. Results are written to `outputs/jarvis.blinded.completion.summary.csv`; the locked JSON artifacts and their hashes use the `locked_jarvis_blind_*` prefix.

The cost-weighted JARVIS companion experiment used the same 187-material intersection and deployment threshold, but expanded the candidate pool with synthetic measured response channels whose cost, benchmark alignment, deployment-residual alignment and noise were controlled. The pool contained a cheap benchmark-aligned probe, a mixed low-cost probe, a low-cost residual probe, a noisy band-gap proxy, an expensive precise residual probe and real MBJ band gap. The completion-per-cost policy maximized the calibration response-rank score divided by declared probe cost; response-rank ignored cost; benchmark-aligned selected maximum formation-energy alignment; uncertainty selected maximum calibration variance; random sampled uniformly; and the oracle-per-cost policy maximized held-out certification gain per cost and is reported only as an upper bound. Outputs are `outputs/jarvis_cost_weighted_probe_pool_summary.csv` and `outputs/jarvis_cost_weighted_probe_pool.pdf`.

**Public finite-fiber audits.** The vision audit used the scikit-learn handwritten-digits dataset and eight classifiers: logistic regression, linear SVM, RBF SVM, random forest, extra-trees,  $k$ -nearest neighbours, a one-hidden-layer multilayer perceptron and Gaussian naive Bayes<sup>1</sup>. Across 25 stratified splits, the benchmark response was clean-image correctness. The deployment response was correctness on the clean image and four deterministic corruptions: Gaussian noise, Gaussian blur, central occlusion and subpixel shift. Finite benchmark fibers were defined by clean predicted class, clean correctness and decile-binned clean confidence. The Tox21 audit downloaded the MoleculeNet CSV from the public DeepChem host, kept compounds with complete labels for seven nuclear-receptor assays and SR-p53, grouped exact assay patterns and classified fibers by unanimity of the held-out endpoint<sup>2</sup>. The spin-defect audit downloaded Toriyama et al. Zenodo data, merged bare-host and heterostructure  $T_2$  records, and classified reported substrate completions under a  $T_2 > 1$  ms viability

threshold<sup>6</sup>. The Matbench audit downloaded public Figshare prediction files and the WBM test-set summary, paired formation-energy predictions with stability labels, and evaluated quantile, nearest-neighbour and error-window fibers<sup>7,8</sup>. The JARVIS audit downloaded public prediction files for formation energy and optB88vdW band gap from the JARVIS-Leaderboard GitHub repository and evaluated an  $E_{\text{gap}} > 1.0$  eV threshold<sup>9</sup>. Continuous audits were reported only after declaring finite resolutions. For Matbench and JARVIS, quantile fibers used 5, 10, 20, 40, 80 and 100 bins; nearest-neighbour fibers used  $k = 10, 25, 50, 100$ ; and error-window fibers used each model’s mean absolute error, 80th-percentile absolute error and 95th-percentile absolute error as tolerances. Supplementary Table 2 reports certifiable fractions, fiber sizes, decision-risk error and normalized residual ambiguity for these declared finite-resolution rules. These tolerance choices audit released predictions; structure and descriptors can be added as richer evidence maps.

# Supplementary information

Domain	Unit $s$	Evidence map $E(s)$	Evidence added only in completion/richer analyses	Deployment action $D(s)$	Fiber rule
Vision	Image-classifier instance	Clean predicted class, clean correctness and clean-confidence decile	Corrupted-image responses	Corruption-robust correctness	Exact finite fibers
Tox21	Compound	Seven nuclear-receptor assay labels	SR assays, molecular structure and fingerprints	SR-p53 label	Exact assay pattern
Spin defects	Host/substrate candidate	Bare-host response	Substrate-specific response	Substrate viability	Reported substrate completions
Matbench	Material-model prediction row	Released formation-energy prediction	Structure, composition, model internals and stability label	Stability decision	Finite-resolution fibers
JARVIS	Material-model prediction row	Released formation-energy prediction	Band-gap probes before completion, structure, composition and model internals	$E_{\text{gap}} > 1.0$ eV	Finite-resolution fibers

**Supplementary Table 1. Evidence maps used in the public audits.** Each row specifies the scored evidence map, the deployment action and the fiber rule. Information outside the scored evidence map can be added as richer evidence or response-completion probes, changing the completion cost.

Domain	Fiber rule	Parameter	Cert. %	IQR %	Median fiber	Decision-risk %	$\rho$
Matbench	Quantile	5	0.00	0.00–0.00	51,391	18.79	1.00
Matbench	Quantile	10	0.00	0.00–0.00	25,696	18.79	1.00
Matbench	Quantile	20	0.00	0.00–0.00	12,848	18.79	1.00
Matbench	Quantile	40	0.00	0.00–0.00	6,424	18.79	1.00
Matbench	Quantile	80	0.00	0.00–0.00	3,212	18.79	1.00
Matbench	Quantile	100	0.00	0.00–0.00	2,570	18.79	1.00
Matbench	kNN	10	25.43	23.95–26.74	10	18.04	0.96
Matbench	kNN	25	13.09	11.43–15.24	25	18.58	0.99
Matbench	kNN	50	8.58	7.09–11.58	50	18.71	1.00
Matbench	kNN	100	5.18	4.38–9.49	100	18.75	1.00
Matbench	Error window	MAE	< 0.01	< 0.01–0.01	196,278	18.95	1.01
Matbench	Error window	80% abs. error	< 0.01	< 0.01–< 0.01	217,152	19.09	1.02
Matbench	Error window	95% abs. error	< 0.01	< 0.01–< 0.01	252,058	18.82	1.00
JARVIS	Quantile	5	0.00	0.00–0.00	1,114	21.55	1.00
JARVIS	Quantile	10	0.00	0.00–0.00	557	19.40	0.90
JARVIS	Quantile	20	0.00	0.00–0.00	279	19.27	0.89
JARVIS	Quantile	40	0.00	0.00–0.00	139	19.10	0.89
JARVIS	Quantile	80	1.26	1.25–2.50	70	18.93	0.88
JARVIS	Quantile	100	2.01	1.50–3.01	56	18.95	0.88
JARVIS	kNN	10	27.08	26.59–27.26	10	17.68	0.82
JARVIS	kNN	25	9.83	8.78–10.97	25	18.57	0.86
JARVIS	kNN	50	2.33	2.00–3.85	50	18.90	0.88
JARVIS	kNN	100	0.00	0.00–0.54	100	19.04	0.88
JARVIS	Error window	MAE	2.64	1.32–3.89	128	18.89	0.88
JARVIS	Error window	80% abs. error	2.19	1.03–3.01	159	18.96	0.88
JARVIS	Error window	95% abs. error	0.74	0.55–1.35	501	19.12	0.89

**Supplementary Table 2. Continuous-fiber decision-risk sensitivity.** Values are medians across 67 Matbench Discovery prediction files or 15 JARVIS public models. IQR denotes the 25th–75th percentile interval across files or models. For quantile fibers, decision-risk error is the Bayes error of the best partition-wise action under the declared evidence rule. For kNN and error-window neighbourhoods, it is local-neighbourhood majority error; because these neighbourhoods overlap and do not define a global partition, the normalized value can slightly exceed one when the local evidence is less informative than the global majority rule. The source table is `outputs/continuous_fiber_decision_risk_summary.csv`.

## Data availability

Public datasets are downloaded or loaded at runtime by the scripts: scikit-learn handwritten digits, MoleculeNet Tox21, Toriyama et al. Zenodo spin-defect data, Matbench Discovery Figshare/WBM test-set files and JARVIS-Leaderboard GitHub files. Numerical summaries cited in the manuscript are cached in `outputs/`. The label-blinded JARVIS replay additionally writes locked probe-order, decision and manifest JSON files with SHA-256 hashes before held-out deployment labels are scored.

## Code availability

The reusable BenchCert tool for deployment-completeness audits is available at <https://github.com/E-zClap/benchcert>. Code to reproduce the analyses, figures and tables in this manuscript is available at <https://github.com/E-zClap/benchcert-reproducibility>. The reproducibility repository includes installation instructions, dependency specifications, scripts for all experiments and cached numerical outputs. The locked JARVIS replay is generated by `scripts/jarvis_blinded_completion_campaign.py`. The command `bash reproduce_all.sh` regenerates the cached outputs and manuscript figures from public data, including the continuous-fiber decision-risk table, prevalence-normalized ambiguity summary, Tox21 selective baseline and asymmetric cost sweep. The cost-weighted JARVIS companion pool is generated by `scripts/jarvis_cost_weighted_probe_pool.py`.

## Acknowledgements

This research was supported by JSPS KAKENHI Grant Number 24K21730.

# Competing interests

The authors declare no competing interests.

## References

- [1] F. Pedregosa, G. Varoquaux, A. Gramfort, V. Michel, B. Thirion, O. Grisel, M. Blondel, P. Prettenhofer, R. Weiss, V. Dubourg, J. Vanderplas, A. Passos, D. Cournapeau, M. Brucher, M. Perrot, and E. Duchesnay. Scikit-learn: Machine learning in python. *Journal of Machine Learning Research*, 12:2825–2830, 2011.
- [2] Z. Wu, B. Ramsundar, E. N. Feinberg, et al. MoleculeNet: a benchmark for molecular machine learning. *Chemical Science*, 9:513–530, 2018.
- [3] D. D. Awschalom, R. Hanson, J. Wrachtrup, and B. B. Zhou. Quantum technologies with optically interfaced solid-state spins. *Nature Photonics*, 12:516–527, 2018. doi: 10.1038/s41566-018-0232-2.
- [4] H. Seo, H. Ma, M. Govoni, and G. Galli. Designing defect-based qubit candidates in wide-gap binary semiconductors for solid-state quantum technologies. *Physical Review Materials*, 1:075002, 2017. doi: 10.1103/PhysRevMaterials.1.075002.
- [5] Michael Y. Toriyama, Jiawei Zhan, Shun Kanai, and Giulia Galli. Strategies to search for two-dimensional materials with long spin qubit coherence time. *npj 2D Materials and Applications*, 9:108, 2025. doi: 10.1038/s41699-025-00623-8.
- [6] Michael Y. Toriyama, Jiawei Zhan, Shun Kanai, and Giulia Galli. Dataset: Strategies to search for two-dimensional materials with long spin qubit coherence time. Zenodo, 2025. doi: 10.5281/zenodo.16996230.
- [7] Janosh Riebesell, Rhys E. A. Goodall, Philipp Benner, Yuan Chiang, Bowen Deng, Gerbrand Ceder, Mark Asta, Alpha A. Lee, Anubhav Jain, and Kristin A. Persson. A

- framework to evaluate machine learning crystal stability predictions. *Nature Machine Intelligence*, 7:836–847, 2025. doi: 10.1038/s42256-025-01055-1.
- [8] Hai-Chen Wang, Silvana Botti, and Miguel A. L. Marques. Predicting stable crystalline compounds using chemical similarity. *npj Computational Materials*, 7:12, 2021. doi: 10.1038/s41524-020-00481-6.
- [9] Kamal Choudhary, Kevin F. Garrity, Andrew C. E. Reid, Brian DeCost, Adam J. Biacchi, Angela R. Hight Walker, et al. The joint automated repository for various integrated simulations (JARVIS) for data-driven materials design. *npj Computational Materials*, 6:173, 2020. doi: 10.1038/s41524-020-00440-1.
- [10] Ronald A. Fisher. On the mathematical foundations of theoretical statistics. *Philosophical Transactions of the Royal Society of London. Series A*, 222:309–368, 1922.
- [11] David Blackwell. Equivalent comparisons of experiments. *The Annals of Mathematical Statistics*, 24(2):265–272, 1953.
- [12] Charles F. Manski. Nonparametric bounds on treatment effects. *American Economic Review*, 80(2):319–323, 1990.
- [13] Charles F. Manski. *Partial Identification of Probability Distributions*. Springer, New York, 2003.
- [14] Elie Tamer. Partial identification in econometrics. *Annual Review of Economics*, 2:167–195, 2010.
- [15] Dennis V. Lindley. On a measure of the information provided by an experiment. *Annals of Mathematical Statistics*, 27(4):986–1005, 1956.
- [16] Ronald A. Howard. Information value theory. *IEEE Transactions on Systems Science and Cybernetics*, 2(1):22–26, 1966.

- [17] Kathryn Chaloner and Isabella Verdinelli. Bayesian experimental design: A review. *Statistical Science*, 10(3):273–304, 1995.
- [18] Friedrich Pukelsheim. *Optimal Design of Experiments*. Society for Industrial and Applied Mathematics, Philadelphia, PA, 2006.
- [19] Tilmann Gneiting. Making and evaluating point forecasts. *Journal of the American Statistical Association*, 106(494):746–762, 2011.
- [20] Nicolas S. Lambert, David M. Pennock, and Yoav Shoham. Eliciting properties of probability distributions. In *Proceedings of the 9th ACM Conference on Electronic Commerce*, pages 129–138, 2008.
- [21] Rafael Frongillo and Ian A. Kash. Vector-valued property elicitation. In *Proceedings of The 28th Conference on Learning Theory*, volume 40 of *Proceedings of Machine Learning Research*, pages 710–727, 2015.
- [22] C. K. Chow. On optimum recognition error and reject tradeoff. *IEEE Transactions on Information Theory*, 16(1):41–46, 1970.
- [23] Y. Geifman and R. El-Yaniv. Selective classification for deep neural networks. In *Advances in Neural Information Processing Systems*, volume 30, 2017.
- [24] V. Vovk, A. Gammerman, and G. Shafer. *Algorithmic Learning in a Random World*. Springer, New York, 2005.
- [25] Jing Lei, Max G’Sell, Alessandro Rinaldo, Ryan J. Tibshirani, and Larry Wasserman. Distribution-free predictive inference for regression. *Journal of the American Statistical Association*, 113:1094–1111, 2018.
- [26] Ryan J. Tibshirani, Rina Foygel Barber, Emmanuel J. Candès, and Aaditya Ramdas. Conformal prediction under covariate shift. In *Advances in Neural Information Processing Systems*, volume 32, 2019.

- [27] D. Hendrycks and K. Gimpel. A baseline for detecting misclassified and out-of-distribution examples in neural networks. In *International Conference on Learning Representations*, 2017.
- [28] Y. Ovadia, E. Fertig, J. Ren, Z. Nado, D. Sculley, S. Nowozin, et al. Can you trust your model’s uncertainty? Evaluating predictive uncertainty under dataset shift. In *Advances in Neural Information Processing Systems*, volume 32, 2019.
- [29] P. W. Koh, S. Sagawa, H. Marklund, et al. WILDS: A benchmark of in-the-wild distribution shifts. In *Proceedings of the 38th International Conference on Machine Learning*, pages 5637–5664, 2021.
- [30] Ishaan Gulrajani and David Lopez-Paz. In search of lost domain generalization. In *International Conference on Learning Representations*, 2021.